
# VLASS Project Memo #13:

# Pilot and Epoch 1 Quick Look Data Release

***M. Lacy, S. Myers, A. Kimball, F. Schinzel, C. Chandler, L. Sjouwerman, J. Marvil, J. Masters, D. Medlin, A. Vargas, K. Radford, A. Sobotka (NRAO)***

***June 30, 2019***

The Very Large Array Sky Survey (VLASS) produces "Quick Look" image products using a simple imaging algorithm as rapidly as possible after the data are taken, in order to enable searches for transient objects. In this Memo we describe and characterize the Quick Look image products from the VLASS pilot survey and the first half of the first epoch of VLASS. At Dec $> -20°$ the error in the source positions is $\approx 0\farcs5$, increasing to $\approx 1''$ at Dec $-40°$. For flux densities below $\approx$ 1Jy, the peak flux densities are systematically low by $\approx 15\%$, and the total flux densities low by $\approx 10\%$, with a systematic scatter of $\approx \pm 8\%$. Above 1 Jy the flux densities can be very unreliable and should not be used. We emphasize that these products are not suitable for use if high flux density and/or positional accuracy are required.

## 1. Introduction

The data release plan for VLASS calls for "Quick Look" (QL) images to be made available within a short timescale of observation (goal of one week, requirement of two weeks) to aid with searches for transients. This memo characterizes the calibration and QL imaging products for the VLASS pilot observations, and the first and second observing sessions that comprise the first epoch of VLASS (VLASS1.1 and VLASS1.2). Future memos will describe the set of higher quality products resulting from Single Epoch and Cumulative Epoch processings, which will use more accurate imaging techniques.

The VLASS pilot survey[1] was executed from June to September 2016. The observations were designed to map key areas needed to inform the final survey design and provide observations of well-studied fields that enable comparison with prior data, both at radio and

[1] `https://go.nrao.edu/vlass-memo002`

other wavelengths. The pilot was also used to test the observing strategy and setup. It used 196 hr of VLA time and covered 2480 $\deg^2$ of sky. The pilot survey includes both single scans and full depth (three repeats within the 4-month duration of the B-configuration in which the pilot was observed) on a set of well-studied fields, selected to contain complementary data at radio and/or other wavelengths. Raw visibility data and calibration products for data taken during the pilot are available for download in the NRAO archive under project code TSKY0001 (see https://science.nrao.edu/science/surveys/vlass/ for information on how to identify the pilot scheduling blocks in the archive). Quick Look images from the pilot are available through the same web interface as the VLASS1.1 and VLASS1.2 Quick Look images.

The first half of the first epoch of VLASS was observed from September 2017 to February 2018, and is stored under project VLASS1.1 in the NRAO archive. The second half of the first epoch began execution in March 2019 (project code VLASS1.2) and ending in July 2019, to complete the first pass of all-sky imaging.

The overall VLASS calibration strategy is described by Lacy et al. (2019). In this memo we first describe specific calibration issues that affected only the pilot and the first epoch of VLASS, then characterize the Stokes I continuum products produced by the QL imaging pipeline.

## 2. Calibration issues specific to the pilot and epoch 1 Quick Look calibration

### 2.1. Antenna pointing corrections

The antenna pointing data recorded in the pointing tables of the raw Science Data Model (SDM) files were incorrect for the pilot survey and for the first half of the first epoch (VLASS1.1). For the pilot processing, the pointing table had erroneous entries and had to be removed completely prior to processing. We expect this to have little impact on QL images as the pointing uncertainty is less than $\approx 0.1$ of the primary beam FWHM. However, during VLASS1.1 all antennas with old-style Antenna Control Units (ACUs, comprising around 2/3 of the antennas during VLASS1.1) were mis-pointed due to an error in the timing for commands sent to those ACUs, and had a pointing table that did not reflect the true pointing direction but only the direction that the executor was using (see VLASS Memo #12[2] for a more detailed description of the problem). This pointing offset affected both derived flux densities and in-band spectral indices. The pointing tables will be corrected before the Single Epoch imaging is undertaken for VLASS1.1. The pointing tables are correct in VLASS1.2, but do need additional processing before they can be used by the imaging algorithms in CASA.

[2]http://go.nrao.edu/vlass-memo012

### 2.2. Delay center errors

Throughout the pilot, VLASS1.1, and VLASS1.2 various online system problems resulted in occasional incorrect delay centers being used by the correlator during parts of an On-The-Fly (OTF) mosaic scan, resulting in the position used by the correlator being different from that recorded in the SDM metadata. These data, when imaged, cause copies (or "ghosts") of any sources in that field to appear, offset from their true positions; see Section 3.2 below for further details of how ghosts are diagnosed and corrected). This problem was first identified early during VLASS1.1 observing by colleagues from Caltech (D. Dong and G. Hallinan), when searching the Pilot and VLASS1.1 for transients compared to the FIRST survey catalog. In some cases, the problem resulted in a characteristic signature in the visibility data, whereby an incorrect number of integrations had been assigned to each phase center (i.e., each Field in the MeasurementSet, or MS). These could be identified and flagged before imaging. However, the majority of cases could only be identified during imaging, with no other signatures seen in the SDM or MS metadata.

The origin of the problem described above was identified and a bug fix deployed in the online system on November 15, 2017. No ghosts of the kind described above were seen for the rest of VLASS1.1. However, the solution introduced a potential race condition where occasionally an incorrect delay model was used 10 seconds into the start of an OTF row, which was only discovered during VLASS1.2 observing and corrected in the online system on June 13, 2019. This problem has likely existed since November 15, 2017.

In addition to the two problems described above, other updates to various components of the online system to try to fix bugs experienced by other (non-VLASS) observers caused ghosts at the start of OTF rows between March 14, 2019 and May 13, 2019 (VLASS1.2). In a very small number of instances in this same time range, a similar effect was seen in calibrator scans with phase jumps usually lasting 10s before returning to nominal phase. These were identified and flagged (and the data re-calibrated, if deemed serious enough to impact QL imaging).

Table 1 summarizes the dates for which various problems relating to delay models were experienced for the pilot, VLASS1.1, and VLASS1.2.

### 2.3. Polarization calibration in the pilot

The pilot survey was observed with full polarization calibration, with the primary position angle calibrator being 3C286. In parts of the sky where 3C286 was not observable, 3C48 was used as polarization position angle calibrator. However, 3C48 is only weakly polarized at the low end of the VLASS observing frequency range. Calibration with 3C48 thus led to higher uncertainties in polarization angle calibration at 2.0–2.5 GHz with uncertainties of up to $\sim 4^\circ$ in absolute position angle. Furthermore, several tiles did not observe the leakage calibrator over a large enough range in parallactic angle to obtain a correct calibration. We therefore do not intend to produce polarization products for the pilot. In VLASS1.1 and VLASS1.2, if 3C286 was not available, one of two secondary polarization calibrators, 3C138

Table 1: Summary of symptoms and dates affected by delay problems in the VLASS pilot, VLASS1.1, and VLASS1.2

| Date range | Symptom |
|---|---|
| Pre-2017 Nov 15 | Ghost sources caused by Executor falling behind sending delay models to correlator (Pilot, VLASS1.1) |
| 2019-Mar-14 through 2019-May-13 | CMIB software update resulted in occasional phase jumps lasting for 10s on calibrator scans, and occasional ghosts at the start of OTF rows (VLASS1.2) |
| 2017-Nov-15 through 2019-Jun-13 | Race condition occasionally caused 11th Field from the start of an OTF row to be correlated at the wrong position (VLASS1.1, VLASS1.2) |

or J1800+7828, were used. The secondary calibrators are variable, and a time-dependent model will be used in the Single Epoch calibration pipeline to deal with this.

## 3. Imaging

VLASS Quick Look Images are produced using the CASA task *tclean* with *gridder='mosaic'* using 1-arcsecond pixels (i.e., the Point Spread Function is under-sampled, and there are no corrections for w-terms). These approximations make the imaging fast, but combined with the non-optimal primary beam models used by this gridder, lead to reduced fidelity for these image products as described in Section 3.3. The images are made as $2\times2$ deg$^2$ mosaics, and are subsequently trimmed down to $1\times1$ deg$^2$ to ensure that sources on the edges of the final image products are correctly deconvolved. More accurate Single Epoch images will be produced later for use in cases where more accurate flux densities and positions are needed. Single Epoch images will also include spectral index information and coarse cubes in Stokes I, Q and U.

### 3.1. Noise images

Root mean square deviation (RMSD) images for estimating the noise as a function of position in the VLASS images are supplied as part of the QL data products. These are generated using the CASA task *imdev*, available in CASA version 5.0.0 and following. This task has a variety of algorithms available for estimating the RMSD from a set of pixel values. The one selected for VLASS was the Chauvenet criterion, which eliminates data points that lie outside the expected range for members of a normal distribution of data points.[3]. The RMSD image is evaluated on a rectangular grid with 20 pixel spacing, using a $60 \times 60$ pixel box (both the grid spacing and box size are configurable in the CASA

[3] `https://en.wikipedia.org/wiki/Chauvenet's_criterion`

task, and a circle can be used instead of a box). A cubic interpolation is used between grid points, and for extrapolation beyond the edge of the grid. (In the case of a cube, the RMSD images are calculated per plane.)

### 3.2. Ghost sources

Ghost sources resulting from erroneous delay centers being used in the correlator (first and second lines of Table 1) are typically faint copies of sources at positions offset by integer numbers of phase centers (Fields) — 178.74 arc-seconds in Right Ascension (RA) for a nominal scan rate of 3.31 arc-minutes/sec and 0.9 second sub-scans. Because the data were correlated at a previous position in the OTF scan but assigned the intended position in the SDM and MS, ghosts appear "ahead" of the true position in the OTF scan direction. Cases of ghosts have been identified with offsets of up to 10 field separations from the correct position, although the predominant offset is a single phase center (i.e., the data were recorded with the preceding delay center).

Ghosts are identified by making initial QL images for an entire tile, after which component lists are created using PyBDSF [1] and searched for fainter sources appearing an integer number of offsets in RA only (with a tolerance of $2''$) from brighter sources. When this is seen, images are made of each phase-center in that region, and fields identified where the ghosts actually occurred. These fields are then flagged in the calibrated MS, and the affected images re-made. In addition, the new flags are saved with the archived calibration so that subsequent restorations of this data will not have these ghosts. Note that the identification of these ghost images requires there to be a sufficiently bright source in the affected fields, above the thresholds chosen in the execution of PyBDSF (5-sigma). Therefore, there are probably residual ghosts remaining in the data and QL images that fall below these thresholds, and caution should be taken when using QL images to search for faint transients.

In addition to the ghosts described above, the race condition (third line of Table 1) sometimes caused the 11th Field from the start of an OTF row to be correlated at the wrong position in a way that was not just an offset in RA, and could be very far from the intended delay center. In these cases, images of the 11th Field typically appear blank (any sources are usually outside the primary beam, but in extreme cases may cause ghosts), while other nearby Fields in the OTF row may contain sources. The effect of the inclusion of these blank fields in the QL images is to slightly depress the flux densities of measured for sources at these locations. The QL images have not been corrected for this problem, but these Fields will be flagged before the production of Single Epoch images.

### 3.3. Quick Look image quality

Quick Look images are relatively fast to produce, but suffer from inaccuracies in both position and flux density, due to the issues described above. In order to quantify the uncertainties in flux density and position in the QL images, we used a number of techniques.

First, we made use of re-observations on individual tiles. Several tiles were covered twice during the VLASS1.1 observations: in one case the Moon was accidentally observed in the tile (T14t05), and two (T09t02 and T09t35) were re-observed due to gain compression from RFI, but were later successfully recovered. In the pilot, several tiles were observed multiple times. For this analysis we used the images made of the Chandra Deep Field South (CDFS), for which an observation tile was repeated three times. These duplicate observations were used for consistency and validation checks on the QL imaging. Second, we matched a catalog generated by PyBDSF over the entire VLASS1.1 dataset to Gaia DR2, to investigate issues with positional accuracy. Third, we compared the flux densities and positions of calibrators recovered from the QL mosaics to their values from the pointed observations used to derive the calibrations. Finally, we also compared the flux densities of less variable calibrators to their values from the literature as a check on the absolute flux density calibration.

### 3.3.1. Quick Look positional accuracy

The catalog from the Quick Look observations of VLASS1.1 was matched to the *Gaia* DR2 release using a $1''$ match radius. 64,647 sources were matched (in 479 cases a VLASS source was matched to more than one *Gaia* source; both possible matches were retained in the catalog). The blue points in Figure 1 shows that there is a significant trend in Declination (Dec) difference with Dec between the sources in the VLASS QL images and their *Gaia* identifications. There seems to be no comparable systematic trend of RA difference with Dec, but it seems that individual tiles show systematic offsets. We also measured the positions of phase calibrators within the QL images and compared to their positions in the VLA calibrator catalog[4]. These are shown as red points in Figure 1, and confirm the trends seen in the match to *Gaia*. There are no clear trends in offsets as a function of RA. Figure 1 indicates that, above Dec $-20°$, the systematic component of the positional offets is $<0\farcs5$, but at lower Decs it can rise to as much as $\approx 1''$.

The CDFS images from the pilot had offsets similar to the VLASS1.1 data. The first and third epochs (taken at a mean Hour Angle (HA) of +2.3 hr) were both offset by 0.0 arcsec in RA and +0.5 arcsec in Dec, while that taken at a mean HA of 3.2 hr had an offset of 0.1 arcsec in RA and 0.3 arcsec in Dec (all offsets in the same sense as Figure 1). This is consistent with the same issues affecting positional accuracy in both the pilot and VLASS1.1 data.

Tests using *gridder='awproject'* and *wprojplanes≥16* show greatly reduced position offsets, suggesting that they are likely due to the wide-field w-term effect adding up over the different fields going into the image. Such an effect would have a Dec and Hour-angle dependence due to the aspect of the array during the OTF snapshots. We are currently investigating this hypothesis.

[4] `http://go.nrao.edu/callist`

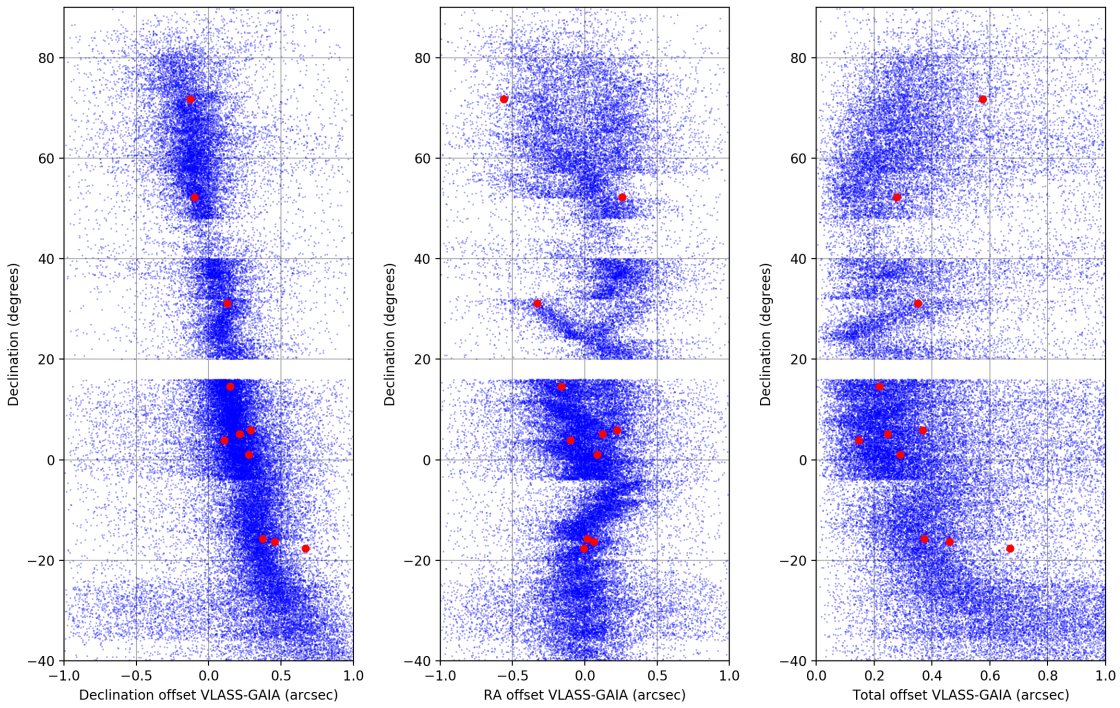


Figure 1: Positional offsets compared to Gaia DR2 (blue points) and VLA calibrator positions from the VLA Calibrator Catalog (red points). *Left:* Declination offset versus Declination, *middle:* Right Ascension offsets versus Declination, *right:* total offset versus Declination.

### 3.3.2. Quick Look flux density accuracy

We compared the measured flux densities of 56 calibrator sources that lie within the VLASS1.1 QL images with their flux densities derived from the pointed calibrator observations made during the observations of the same scheduling blocks. Any differences in the recovered flux densities should thus be dominated by the effect of the QL imaging algorithm and the online pointing offset bug that affected only the OTF data. As Figure 2 shows, there is a systematic offset of about 15% in peak flux densities and 10% in total flux densities between the calibrator flux density measurements as derived from the pointed calibration observations, and those measured (using the CASA *imfit* task) in the QL images, in the sense that the QL flux densities are low.

To quantify issues with fainter sources, the peak flux densities in the QL images of the two VLASS1.1 observations of the tile T14t05 were compared. This comparison showed a scatter in the ratio of peak flux densities with a systematic periodicity with Dec at about the 15% level, with a period corresponding to about the primary beam FWHM. No such trend is seen in the ratio of total flux densities, but again, even for bright sources, the flux densities have a scatter of about 15%.

The ratio of peak flux densities of sources observed in the repeat observations that comprise the pilot data in CDFS shows no periodicity with Dec, and the scatter shows a significantly lower level of systematic uncertainty, with only 5% scatter in the flux ratios for objects with flux densities >10 mJy. In terms of overall offsets, the flux densities of the first and third epochs of the CDFS field (which were taken at close to the same hour angle) are the same to within 1%, however, those in the second epoch are lower by about 8% than those in the first and third epochs. The cause(s) of the effects described above are under investigation.

In order to check the overall flux density scale, a comparison of the flux densities of six calibrators in a Australia Telescope Compact Array (ATCA) calibrator monitoring program [3] that had low variability at 2.5 GHz ($\leq 3\%$) and were present in the VLASS1.1 QL images (J0503+0203, J1150−0023, J1501−3918, J2110−1020, J2129−1538 and J2346+0930) was performed. The mean flux ratio between the VLASS flux densities and those of the ATCA calibrators is 0.98±0.04 (after correction of the 2.5 GHz fluxes to 3.0 GHz using the spectral indices in [3]) with a range of 0.84–1.13. These observations were calibrated using observations of PKS 1934−638, using its flux density from Reynolds (1994)[5].

These comparisons show that there are significant uncertainties associated with the flux densities derived from the QL images, both in terms of scatter ($\approx 15\%$) and an average offset relative to the current Perley-Butler flux density scale [2] of $\approx 10\%$, in the sense that the recovered flux densities from the QL images are (on average) low.

[5] `http://www.atnf.csiro.au/observers/memos/d96783~1.pdf`

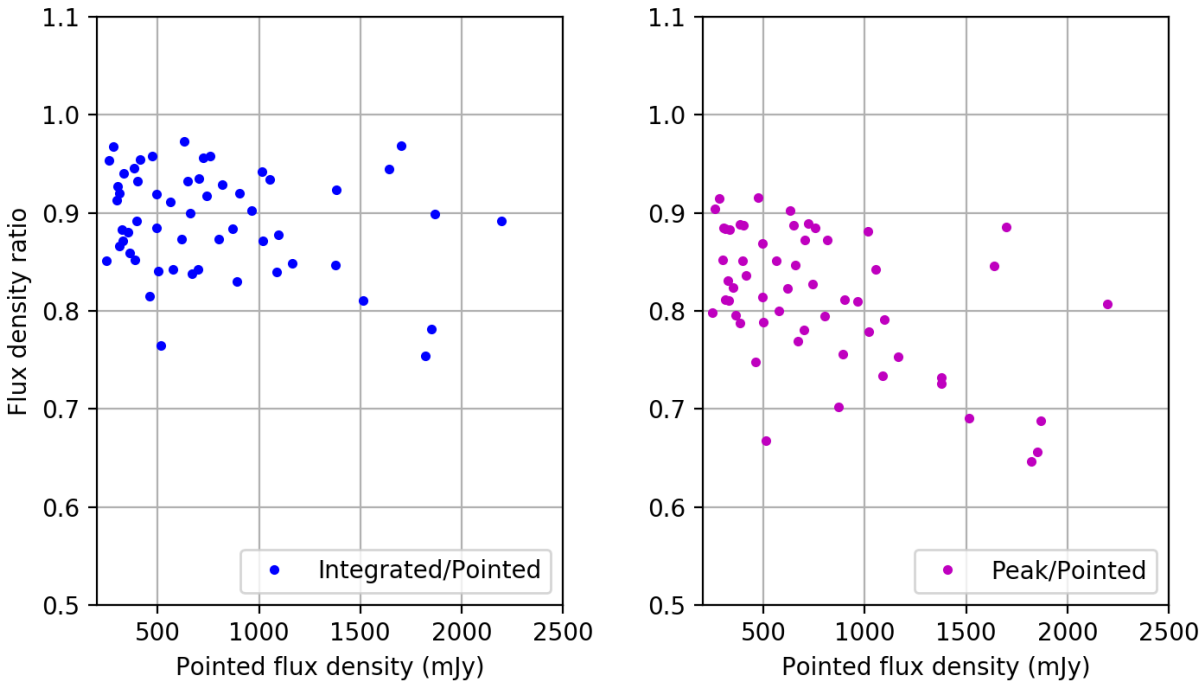


Figure 2: Ratios of measured flux densities on QL images to flux density estimates based on the pointed observations of the calibrators used for gain calibration. *Left:* the ratios of integrated flux densities from the QL images to the pointed values, *right:* the ratios of peak flux densities relative to the pointed values.

### 3.3.3. Sensitivity

The effective integration time for a given position on the sky for VLASS is 5 seconds; taking into account the measured System Equivalent Flux Density (SEFD) across the 2–4 GHz band, and assuming 1500 MHz of RFI-free bandwidth, the theoretical sensitivity should be $\sim$120 $\mu$Jy/beam. Taking into account the approximations used when creating the QL images, the survey system requirement is for the RMS noise in the QL images to be better than 200 $\mu$Jy/beam over at least 80% of the observed sky. Using the noise images described in Section 3.1 we find that for VLASS1.1 this requirement is met for 96% of the observed sky, and furthermore, that 93% of the pixels are within 40% of the theoretical sensitivity (i.e., less than 168 $\mu$Jy/beam).

## 4. Summary

The Quick Look image products from the VLA Sky Survey are designed for transient identification, and, due to the approximations used to construct the images, do not have the accuracy in position or flux density that the final survey products will have. In addition, a problem with the antenna pointing information in VLASS 1.1 added further to systematic errors in the flux densities for those observations. In summary, for Dec $> -20^\circ$ the positional accuracy is $\approx 0\farcs5$, increasing to $\approx 1''$ at Dec $-40^\circ$. For flux densities below $\approx$ 1Jy, the peak flux densities are systematically low by $\approx$ 15%, and the total flux densities by $\approx$ 10%, with a systematic scatter of $\approx \pm 8\%$. Above 1 Jy the flux densities can be very unreliable and should not be used.

## References


[1] N. Mohan and D. Rafferty. PyBDSF: Python Blob Detection and Source Finder. Astrophysics Source Code Library, February 2015.

[2] R. A. Perley and B. J. Butler. An Accurate Flux Density Scale from 50 MHz to 50 GHz. *The Astrophysical Journal Supplement Series*, 230:7, May 2017.

[3] S. J. Tingay, D. L. Jauncey, E. A. King, A. K. Tzioumis, J. E. J. Lovell, and P. G. Edwards. ATCA Monitoring Observations of 202 Compact Radio Sources in Support of the VSOP AGN Survey. *Publications of the Astronomical Society of Japan*, 55:351–384, April 2003.